A nice review of chemistry issues for hypersonics. Most recent known to me. See paper for details. 308 references.

PERGAMON

Progress in Aerospace Sciences 36 (2000) 281–349

PROGRESS IN AEROSPACE SCIENCES

www.elsevier.com/locate/paerosci

Physico–chemical modelling in hypersonic flow simulation

G.S.R. Sarma*

Division of Aerothermodynamics, DLR, Institute for Fluid Mechanics, Bunsenstraße 10, D-37073 Göttingen, Germany

Abstract

The rapid and significant advances in computational power both in terms of hardware and software in recent years and the resurgence in 1980s of interest in future concepts for hypersonic transportation systems and ongoing studies such as those for the International Space Station, Shuttle-like orbital vehicles (Japanese HOPE), reusable launch vehicles (NASA X-33, X-34), and crew rescue vehicles (NASA X-38) have identified CFD as an important and indispensable tool for R & D in the field. To take advantage of this valuable tool for reliable simulations and predictions one must pay careful attention to the quality and validity of the modelling inputs that go into the development of the CFD codes while striving to improve their numerical accuracy and algorithmic efficiency. A review of the governing equations, boundary conditions and the associated inputs by way of physico–chemical models and their partially successful application is given. Some of the 'rate-limiting' steps in achieving predictive capability via CFD are related to inadequacies in the physico-chemical models and in associated data used in describing the multi-species high-temperature chemically reacting gas flows occurring in and around hypersonic vehicles. A few of these continuing modelling challenges are briefly reviewed here with typical examples from current literature.

Regions with chemical and thermal nonequilibrium	
Region	Aerothermal phenomenon
Ⓐ	Chemical and thermal equilibrium
Ⓑ	Chemical nonequilibrium with thermal equilibrium
Ⓒ	Chemical and thermal nonequilibrium

Chemical species in high-temperature air		
Region	Air chemical model	Species present
I	2 species	O_2, N_2
II	5 species	O_2, N_2, O, N, NO
III	7 species	$O_2, N_2, O, N, NO, NO^+, e^-$
IV	11 species	$O_2, N_2, O, N, NO, O_2^+, N_2^+, O^+, N^+, NO^+, e^-$

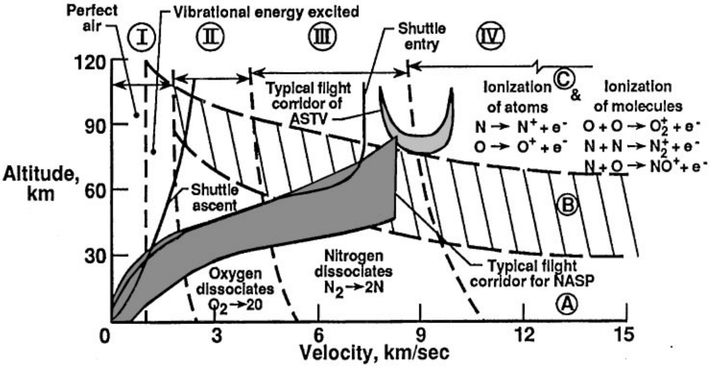

Fig. 1. Flow régimes and thermochemical phenomena in the stagnation region of a 30.5 cm radius sphere flying in air (after [178]).

European high enthalpy wind tunnel capabilities

TH2 is the shock tunnel at Aachen

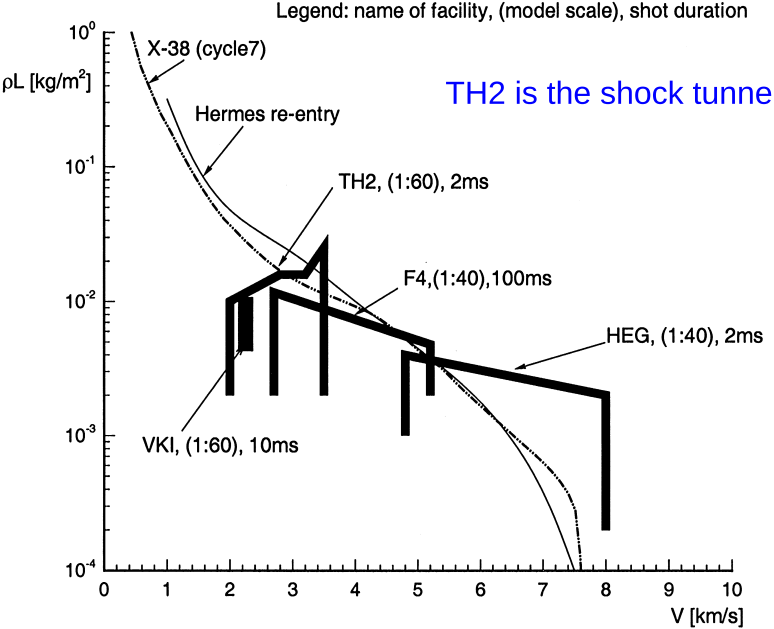

Fig. 2. Testing ranges of some facilities (after [46]). Bold lines indicate the individual range of each facility. Note that the times given are maximal run times and not necessarily testing times for constant conditions in all cases.

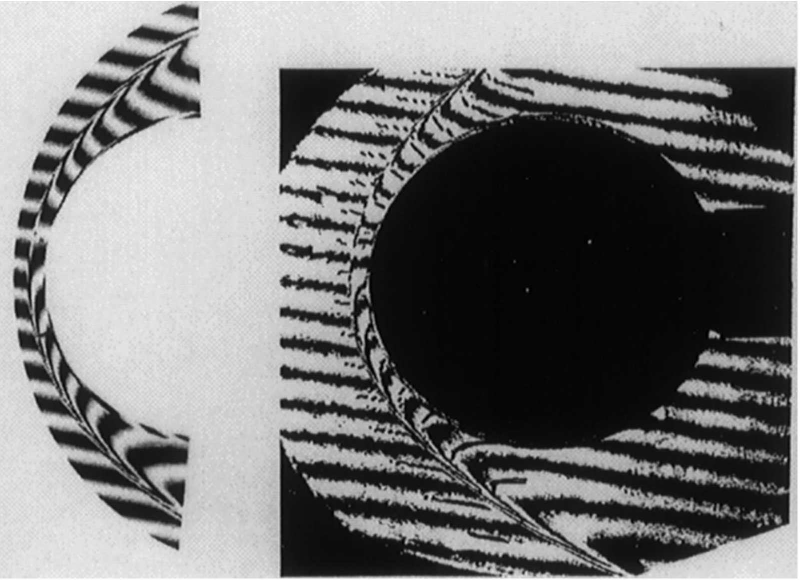

Fig. 7. Comparison of finite-fringe differential interferograms: computed (left) and observed (right) in T5-air flow experiments on a sphere $\varnothing = 4$ in, at $h_0 = 16\,\mathrm{MJ/kg}, p_0 = 27.5\,\mathrm{MPa}$ (after [151], Photo courtesy of Dr. C.-Y. Wen).

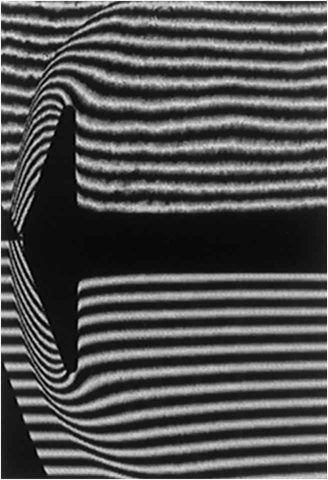

P0=95MPa
H0=
11.6MJ/kg,
T0=6900K

Fig. 12. Interferograms of air flow past 70°-blunted cone at condition VI (top: HEG experiment; bottom: computation) [156].

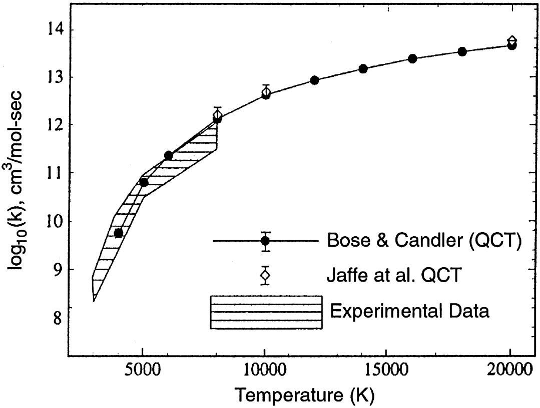

Fig. 26. Total thermal rate constant for $N_2 + O \rightarrow NO + N$: QCT computation and experimental data (after [195]).

Significant differences in rates between quantum computation and old expt data

Table 2
Reaction rate coefficient $k_f(T)$ for $N_2 + O \rightarrow NO + N$ from QCT-fit [190] and empirical fit [187], given in $cm^3/mol^1/s^1$

Temperature T (K)	Bose–Candler QCT $5.69 \times 10^{12} T^{0.42} \times \exp(-42938/T)$	Park et al. $6.4 \times 10^{17} T^{-1.0} \times \exp(-38370/T)$
3000	9.99×10^{07}	5.95×10^{08}
6000	1.71×10^{11}	1.78×10^{11}
10 000	3.72×10^{12}	1.38×10^{12}
14 000	1.46×10^{13}	2.95×10^{12}
18 000	3.21×10^{13}	4.22×10^{12}

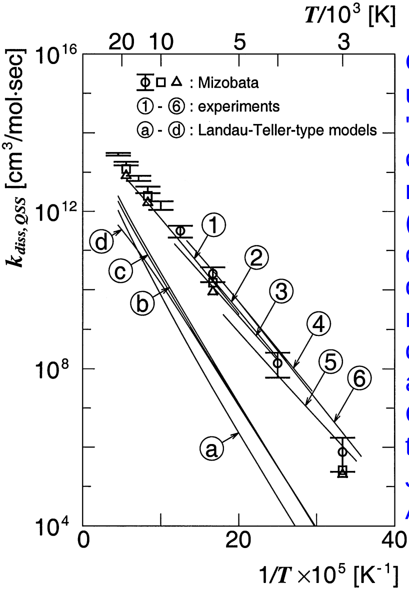

Commonly used 'ladder-climbing' models (a-d) for chemistry do not match expt data. See also Candler's talk from June 2007 AIAA mtg

Fig. 27. Steady-state dissociation rate coefficients for oxygen highly diluted in argon. Experiments by various authors are denoted by circled numerals **1** to **6**. Circled letters **a** to **d** denote various high vibrational bias models. Squares and triangles, respectively denote calculations with softer Lennard–Jones potentials for O–Ar with the short-range exponent changed to 8 (squares) and to 4 (triangles), after Mizobata [199].

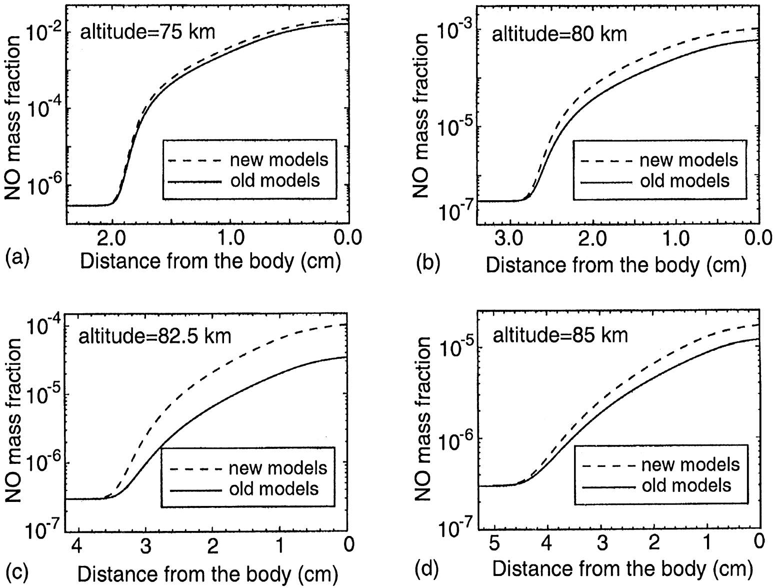

Change in rate constants and details of chemistry models make a big difference (note log scales)

Fig. 31. NO-production along stagnation line in a 5.1 km/s flow past a 10.16 cm radius sphere at various altitudes (after [190]).

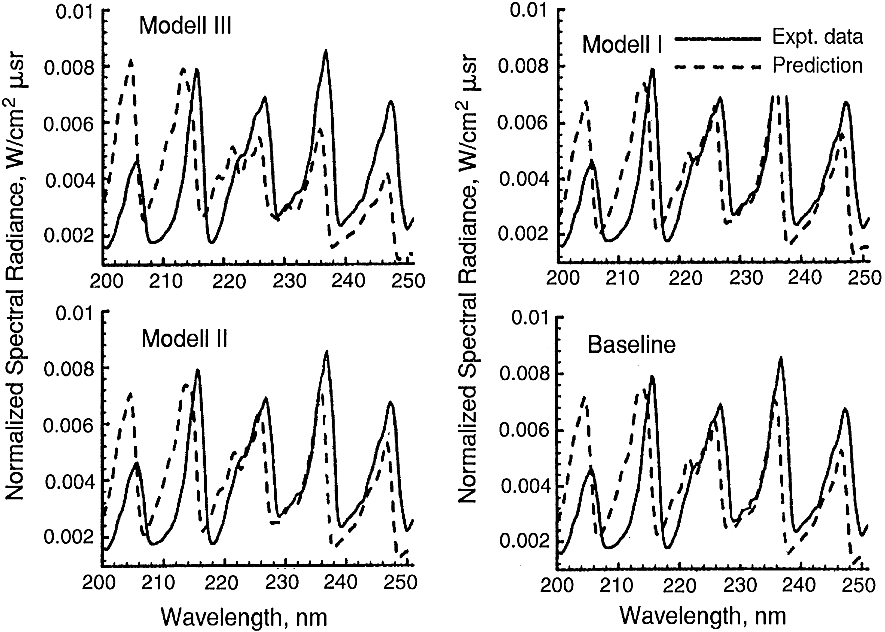

Fig. 32. Computed and BSUV1-experimental stagnation line spectra at 53.5 km altitude (after [193]).

Various chemistry models cp. to flight spectroscopy measurements. Agreement is reasonable but much remains to be done, much uncertainty

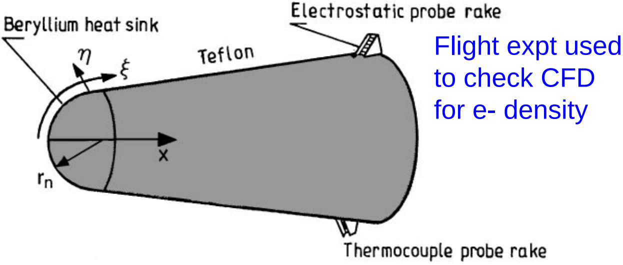

Fig. 46. Schematic of RAM-C II (Radio attenuation measurement); nose-radius, $r_n = 15\,\text{cm}$, cone semi-angle 9°, length 130 cm.

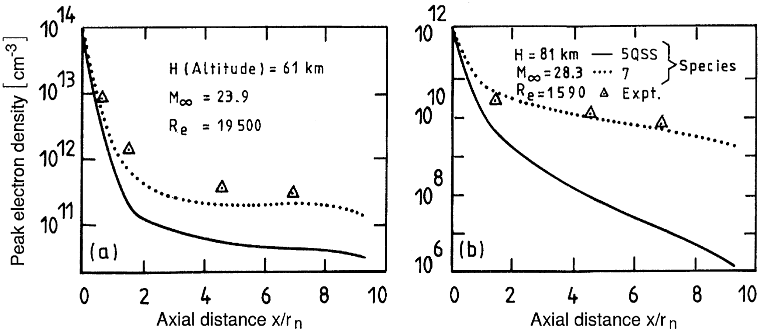

Good agreement under nonequil. conditions at 81km using 7-species model.

Fig. 47. Effects of ionization on peak electron number density at two altitudes, (a) 61 km; (b) 81 km: CFD prediction and flight data for RAM-C II (after Candler [39,235]).

Poor agreement in 48a assumed to be due to uncertainty in the boundary conditions. A fixed wall temp. and noncatalytic wall for electron-ion recomb. may be poor assumptions

See also 'Rate Effects in Hypersonic Flows' by G. Candler, Ann. Rev. Fluid Mech. v. 51, pp. 379-402, 2019.

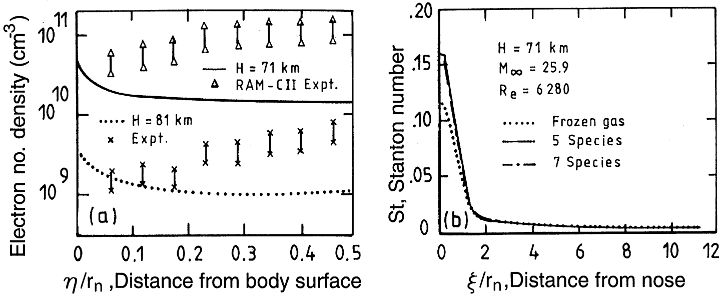

Fig. 48. Effects of ionization on (a) electron number density at $x/r_n = 8.1$; (b) $\mathrm{St} = q_n/\rho_\infty u_\infty(h_\infty - h_w)$: CFD prediction and flight data for RAM-C II (after Candler [39,235]).